Journal of Power Sources 196 (2011) 405–411

Contents lists available at ScienceDirect

Journal of Power Sources

journal homepage: www.elsevier.com/locate/jpowsour

Percolation–tunneling modeling for the study of the electric conductivity in $LiFePO_4$ based Li-ion battery cathodes

Ali Awarke[a,*], Sven Lauer[b], Stefan Pischinger[a], Michael Wittler[a]

[a] Institute for Combustion Engines, RWTH Aachen University, Schinkelstrasse 8, D-52062 Aachen, Germany
[b] FEV Motorentechnik GmbH, Neuenhofstrasse 181, D-52078 Aachen, Germany

ARTICLE INFO

Article history:
Received 21 May 2010
Received in revised form 2 July 2010
Accepted 17 July 2010
Available online 22 July 2010

Keywords:
Li-ion
Cathode
Conductivity
Percolation
Tunneling
$LiFePO_4$

ABSTRACT

In this work a percolation–tunneling based model is developed and used to study the electrical conductivity of $LiFePO_4$ composite Li-ion battery cathodes. The active and conductive additive particles are explicitly represented using a random hybrid geometric-mechanical packing algorithm, while the inter-particle electric transport is achieved by including electron tunneling effects. The model is adjusted to the experimental data of a PVDF/C composite with different mixing ratios. The performed study aims to capture the variation of the conductivity of the $LiFePO_4$ cathode with particle sizes, carbon black particles wt.% and carbon coating wt.%. It is found that ultra fine carbon-free nanosized particles (~50 nm), which are favorable for improved diffusion, would require a relatively high amount of carbon black (15 wt.%) putting at risk the gravimetric capacity of the cell. On the other hand, particles with 1 wt.% continuous carbon coating delivers already sufficient conductivity for all particle sizes without any additives. The further addition of conductive phases is at the risk of redundancy in view of conductivity enhancements. Although continuous carbon coating with loading as low as 1 wt.% is thought to be the most efficient way to achieve electric conductivity, its manufacturability and effect on Li ion diffusion remain to be assessed.

1. Introduction

A trump card in fostering the commercialization of Li-ion based future drive concepts (EV/PHEV) is to replace the expensive conventional $LiCoO_2$ positive active material (AM) in the underlying Li-ion cell [1]. $LiFePO_4$ has been recently suggested [2] due to its low cost, high theoretical capacity, stability and low toxicity, all highly required in vehicle applications. Unfortunately, low Li ionic diffusivity and electric conductivity are two intrinsic features culpable for a high overpotential and thus a limited high rate vehicle performance. Still, the use of nanosized $LiFePO_4$ particles [3,4] which results in shorter diffusion distances, and the addition of conductive particles (mainly carbon black CB) which increases the conductivity several orders [6–11] has paved the way for $LiFePO_4$ into commercial traction applications [5]. So far CB amounts ranging between 2 wt.% and 30 wt.% have been used [10]. Additionally, a carbon coating on the $LiFePO_4$ particles surface [6,12–14] has been applied and found favorable. The indispensable addition of conductive phases may however reduce volumetric and gravimetric energy densities by amounts which are detrimental for EV/PHEV applications [8]. The reason is that the conductive phase does not participate in any electrochemical kinetics and takes the place of the energy producing $LiFePO_4$ active materials. An increase in conductive additive may also cause the decomposition of electrolyte solvent [15,16] as well as reduce the ionic conductivity of the cathode. It is thus important to find an efficient amount of conductive additives, and simulation is indeed a cost-time effective method to realize this goal.

To the best of our knowledge and till the date of this writing, theoretical conductivity investigations on Li-ion composite cathodes are few and accompanied by limiting assumptions. The selection of suitable conductivities has been largely based on approximate calculations using volume fractions [17] and common experimental practices [18]. In [19] an electrode normalized resistance is calculated using an equivalent circuit model assuming finite wiring topologies. It appears that Sastry's group (University of Michigan) is the first to analyze the effective conductivity by modeling the detailed architecture of the underlying cathode microstructure and has performed grueling conductivity investigations on three cathode materials [20]. The particles are nevertheless assumed to be fused resulting in a null contact resistance, and the sizes considered are of the order of several micrometers, which allowed the

Abbreviations: USABC, US advanced battery consortium; EV, electric vehicle; PHEV, pug-in hybrid electric vehicle; AM, active material; CB, carbon black; CNC, carbon nano-coat; RVE, representative volume element; DoE, design of experiment; PVDF, polyvinylidenfluorid; FE, finite element.

* Corresponding author. Tel.: +49 241 5689 379; fax: +49 241 5689 7379.
E-mail address: awarke@vka.rwth-aachen.de (A. Awarke).

0378-7753/$ – see front matter © 2010 Elsevier B.V. All rights reserved.
doi:10.1016/j.jpowsour.2010.07.048

Nomenclature

J	inter-particle current density ($A\,m^{-2}$)
ϕ	electric potential (V)
σ_g	gap conductance ($S\,m^{-2}$)
w	gap thickness (nm)
d	tunneling range (nm)
σ_0	material proportionality constant ($S\,m^{-2}$)
T	temperature (K)
k	Boltzmann constant ($J\,K^{-1}$)
ΔH	activation energy (J)
σ_{eff}	effective conductivity ($S\,m^{-1}$)
wt.%	percentage by weight
vf.%	percentage by volume

assumption of the CB as a homogeneous coating (with the binder) on the particles. Current high rate applications requires $LiFePO_4$ particle to be at the nanoscale. The AM particle size is thus in the range of that of the CB and the dispersion of each phases within each others should be considered in addition to any carbon coating on the AM.

2. Current work

In this work, we model the effective electric conductivity of a $LiFePO_4$ based Li-ion cathode, by referring for the first time to a tunneling–percolation [21,22] theory summarized as follows. When the volume fraction of the conductive clusters is below a percolation threshold, the effective electric conductivity is low and equivalent to the insulating media. Above the percolation threshold an electrically connected continuous conductive network is formed and an abrupt change to a good transport behavior occurs. The resulting effective electric conductivity can yet be several orders less than that of carbon black due to the existence of the insulating binding polymer layer separating the conductive aggregates. This layer is permeable to electrons through the so called tunneling effect[1] [22]. The effective electric conductivity is in the end a result of a combined tunneling–percolation feature in the cathode microstructure. In pure percolation systems the conductivity follows a classical power law with a universal material independent exponent ($t \sim 2$) [23]. On the contrary, in percolation–tunneling systems local tunneling effects result in a non-universal conductivity exponent ranging from 1 to 12 with less than 50% concentration near 2 [24]. The need to consider the morphology of the cathode particulate system and its internal contact features in the electrical conductivity analysis is thus evident. Our modeling is based on tunneling studies for carbon–polymer composites [24–27] which attempt to understand the non-universalities of the conductivity exponent, in addition to a 3D extension of the particle interaction model developed in [28,29].

Tunneling–percolation effects are implemented in a 3D finite element (FE) model of a representative volume element (RVE) resolved at the particle scale and used to analyze the sensitivity of the conductivity to the thickness of carbon coating, CB additive weight fraction and AM particle size. The designated RVE is designed to capture the major feature of the underlying microstructure and is generated using a particle packing procedure elaborated in the next section. The equivalent conductivity of the RVE is extracted numerically using a FE electric transport analysis as shown in Section 4, while the procedure is validated in Section 5 against measurement on a PVDF-CB composite with different volume ratios. In Section 6, we use our validated procedure to perform a design of experiments (DoE) to quantify the effects of the above mentioned factors, while the results are discussed in Section 7. Finally, a conclusion is included in Section 8.

[1] In quantum mechanics "tunneling effect" refers to the penetration of a particle through the potential barrier even if the particle total energy is less than the barrier height.

3. Microstructure generation in a RVE

In order to evaluate the electric conductivity of the cathode composite, virtual electric testing is performed on a material sample volume which is packed with particles and referred to as the RVE. Homogenization theories [30] have shown that the RVE should be typical of the whole mixture on average and contains a sufficient number of inclusions, i.e., the size of the RVE is sufficiently larger than that of the particles. This prerequisite has been minded during each analysis and a minimum safe value of 3.0 [20] is used for the RVE size to particle size ratio.

The packing of particles in a RVE has been the concern of many researches in multi-disciplinary fields. We can distinguish between geometrical [31], mechanical [32,33] and image based [34–36] methods. Given that image based approaches are very expensive to apply, and the limitations of the all alone standing geometrical methods in achieving realistic packing in terms of porosity and contact features, a hybrid geometrical–mechanical algorithm is followed in this work. Starting from the known wt.%, material densities, porosity, distribution in sizes and shapes (aspect ratios), the algorithm calculates the vf.% of each constituent. For the AM and CB additive, ellipsoid with defined aspect ratios and size distribution can be assumed to represent the particles shape. The binder is known to form thin non-continuous layers absorbed on the particles surface [18,37,38], free phases in interstitial sites [39] and bridges connecting particles [40]. Currently, modeling the geometry of the binder phase is an extremely difficult task and can only be processed using imaged based approaches. Considering such difficulty and the fact that the binder is a good insulator, the binder phase will not be modeled while its volume is accounted for by increasing the voids volume fractions. The particle packing algorithm goes as follows. Given the different volume fractions and size distributions, the number of particles in each phase is calculated. In a predefined RVE, particles are randomly inserted one at a time. Overlapping is avoided by repeating an insertion attempt where the inserted particle is found to intersect previously positioned ones. The size of the RVE in the vertical z direction is increased when an insertion attempt failed for 1000 times due to any high specified material concentration.

The above geometrical algorithm is implemented in MATLAB [41] and results in a RVE with non-overlapping non-contacting particles. In highly dense systems with volume fractions approaching the jamming fraction (0.64 for a Random Close Packing of spheres [31]), desired porosity is generally not achieved due to the expansion in the RVE volume, which urges the need for a further densification step using a mechanical finite element simulation as follows. The particles are meshed using a special technique that maps a template mesh to each particle. The discretized particles in addition to the RVE walls are then imported as rigid bodies into a mechanical dynamic analysis using ABAQUS/EXPLICIT [42]. Contact definitions between exposed surfaces are defined and their associated constraints are enforced using the robust penalty method on the expense of slight surface penetrations at equilibrium. During the analysis, the previously adjusted RVE wall surface is assigned a velocity in the direction of decreasing the RVE to its originally assigned size so that the desired porosity is recovered. The whole process is summarized in Fig. 1.

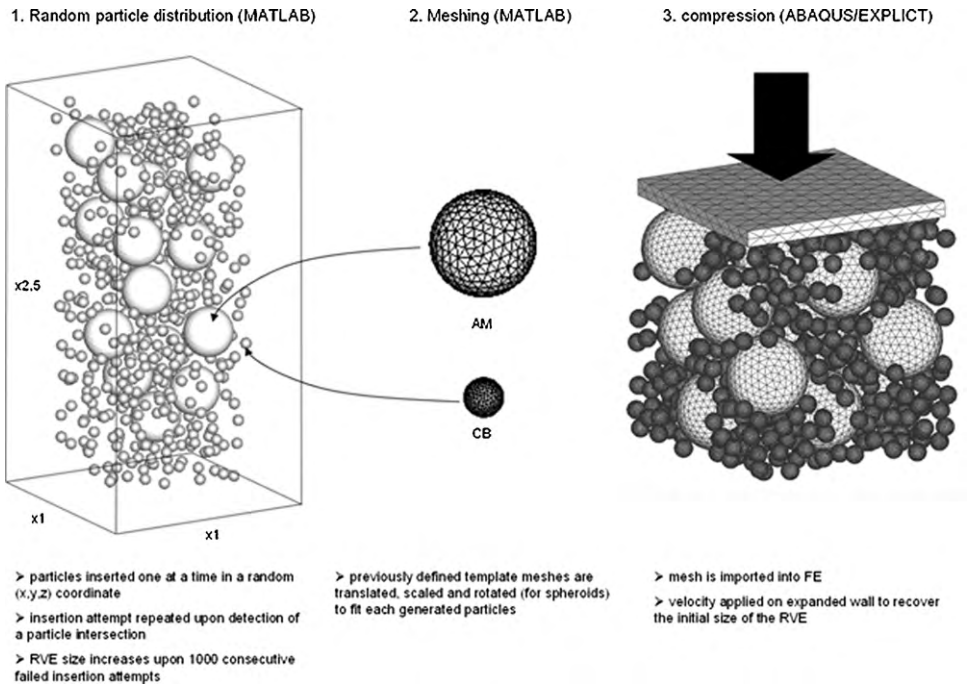

Fig. 1. A comprehensive picture of the RVE generation process.

4. Effective conductivity extraction

The resulting mesh in the above dynamic analysis is imported into a FE electric analysis in ABAQUS/STANDARD [42] where the governed differential equation is the continuity of charge using Ohm's law for the description of the electric current flux. The electric analysis serves as a virtual test to quantify the apparent equivalent conductivity of the composite RVE sample. Bulk electrical conductivities are applied to each phase. The resulting tunneling resistance is modeled by assigning an interfacial contact gap conductance such that the current flowing between two electrically interacting points A and B on two separate particles nearby surfaces is calculated in terms of the potentials at these two points as:

$$J = \sigma_g(\varphi_A - \varphi_B)$$

where J is the inter-particle current density, A m^{-2}; φ is the electric potential, volt; σ_g is the gap conductance, S m^{-2}.

The gap conductance has been found to vary exponentially with the clearance gap [18,24,25,27,43] as:

$$\sigma_g \alpha \exp\left(-\frac{w}{d}\right)$$

where w is the gap thickness and d is the tunneling range. This correlates with the fact that the probability of the electron jumping the gap decreases rapidly with increasing the gap width beyond the tunneling range [43]. Moreover, gap conductance increases exponentially with temperature following an Arrhenius law [22,43], such that the final expression could be written as:

$$\sigma_g = \sigma_0 \exp\left(-\frac{w}{d}\frac{\Delta H}{kT}\right)$$

where σ_0 is a material proportionality constant, S m^{-2}; T is the temperature, K; k is Boltzmann constant, J K^{-1}; ΔH is the activation energy, J.

To extract the effective electric conductivity of the whole system, a unit electric potential difference is applied on two opposite wall surfaces of the RVE, resulting in an effective electric current density (J_{eff}) normal to the two opposite cross sectional areas. Knowing that all other surfaces are insulated and using Ohm's law the effective conductivity σ_{eff} is calculated as:

$$\sigma_{eff} = J_{eff} L \left[\frac{1}{\text{volt}}\right]$$

where L is the size of the RVE.

5. Calibration and validation

To validate our modeling concept, electric conductivity measurements done in [20] on a CB-PVDF composite with different volume ratios are used. Fig. 2 shows the measured variation of the conductivity with the polymer–CB ratio. The witnessed decrease in conductivity with polymer loading is associated with the decrease of CB percolation as well as the increase of the insulating layer between the CB particles. We try in our work to replicate this trend using the above developed modeling procedure and targeting the conductivities at 1.22, 2.74 and 5.48 PVDF/CB volume ratios.

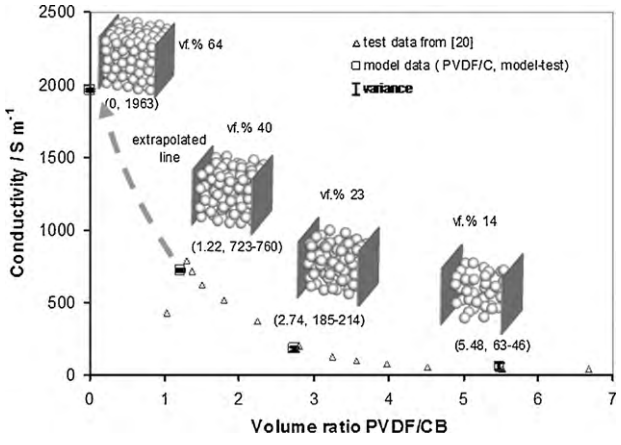

Fig. 2. Test and model conductivity data as a function of PVDF/C volume ratio.

Table 1
Summary of performed experiments.

Exp.	AM size (nm)	CB (wt.%)	Surface carbon (wt.%)	RVE size (nm)	AM (vf.%)	CB (vf.%)	Carbon coat thickness (nm)	Conductivity ($S\,m^{-1}$)
1	50	0.00%	0.00%	150	40.83%	0.00%	0	×
2	100	0.00%	0.00%	300	40.83%	0.00%	0	×
3	200	0.00%	0.00%	600	40.83%	0.00%	0	×
4	50	5.00%	0.00%	150	37.12%	4.05%	0	×
5	100	5.00%	0.00%	300	37.12%	4.05%	0	×
6	200	5.00%	0.00%	600	37.12%	4.05%	0	×
7	50	10.00%	0.00%	150	33.68%	7.81%	0	×
8	100	10.00%	0.00%	300	33.68%	7.81%	0	2.42E−02
9	200	10.00%	0.00%	600	33.68%	7.81%	0	1.62E+00
10	50	15.00%	0.00%	150	30.47%	11.31%	0	2.57E+01
11	100	15.00%	0.00%	300	30.47%	11.31%	0	2.78E+01
12	200	15.00%	0.00%	600	30.47%	11.31%	0	1.41E+01
13	50	0.00%	1.00%	150	40.83%	0.00%	0.15	1.54E+02
14	100	0.00%	1.00%	300	40.83%	0.00%	0.31	1.29E+02
15	200	0.00%	1.00%	600	40.83%	0.00%	0.62	8.95E+01
16	50	5.00%	1.00%	150	37.12%	4.05%	0.15	1.85E+02
17	100	5.00%	1.00%	300	37.12%	4.05%	0.31	3.92E+01
18	200	5.00%	1.00%	600	37.12%	4.05%	0.62	1.06E+02
19	50	10.00%	1.00%	150	33.68%	7.81%	0.15	2.19E+02
20	100	10.00%	1.00%	300	33.68%	7.81%	0.31	1.18E+02
21	200	10.00%	1.00%	600	33.68%	7.81%	0.62	1.27E+02
22	50	15.00%	1.00%	150	30.47%	11.31%	0.15	2.30E+02
23	100	15.00%	1.00%	300	30.47%	11.31%	0.31	2.20E+02
24	200	15.00%	1.00%	600	30.47%	11.31%	0.62	1.54E+02
25	50	0.00%	3.00%	150	40.83%	0.00%	0.46	3.36E+02
26	100	0.00%	3.00%	300	40.83%	0.00%	0.92	2.87E+02
27	200	0.00%	3.00%	600	40.83%	0.00%	1.84	2.09E+02
28	50	5.00%	3.00%	150	37.12%	4.05%	0.46	3.68E+02
29	100	5.00%	3.00%	300	37.12%	4.05%	0.92	5.18E+01
30	200	5.00%	3.00%	600	37.12%	4.05%	1.84	2.25E+02
31	50	10.00%	3.00%	150	33.68%	7.81%	0.46	4.01E+02
32	100	10.00%	3.00%	300	33.68%	7.81%	0.92	1.67E+02
33	200	10.00%	3.00%	600	33.68%	7.81%	1.84	2.28E+02
34	50	15.00%	3.00%	150	30.47%	11.31%	0.46	4.09E+02
35	100	15.00%	3.00%	300	30.47%	11.31%	0.92	3.68E+02
36	200	15.00%	3.00%	600	30.47%	11.31%	1.84	2.54E+02

Due to the lack of details regarding the manufacturing procedure or final microstructure of the considered PVDF/CB composite samples some assumptions will be made as follows. CB particles are represented as spheres with a homogenous diameter of 40 nm which is in agreement with the sizes of commonly observed elementary particles using electron micrographs [18,44,45]. Elementary particles tend to fuse to form larger primary aggregates under different shapes [18,45]. Due to the lack of such description combined with a modeling difficulty in generating fused aggregates, it is assumed in our simulations that during mixing and high densification the aggregates break into their original elementary particles [18] resulting in a random uniform dispersion of CB in its vehicle. Because the PVDF can reside in interstitial sites, the porosities of a PVDF/C system can reach low values. 10% porosity has been assumed which still guaranteed in the densest CB case, a vf.% of CB particles below the jamming fraction (0.64 for a random close packing of spheres). A 10% porosity has also been reported in [18] for different polymer–CB mixtures. A whole amorphous carbon phase is assumed in the CB particles with an electric conductivity of 30,000 $S\,m^{-1}$ [46]. Temperature effects are ignored in all gap conductance calculations in this work. A density of 1.94 $g\,cm^{-3}$ is assumed applicable to the CB particles [18]. The application of continuum mechanics principles at this small scale is also assumed valid given that the lower limit is around 3–5 nm [47].

The fitting parameters are the proportionality constant σ_0 and the tunneling range d. The effective conductivity of neat CB σ_{eff}^{neat} (in the absence of PVDF) can be read as ~1900 $S\,m^{-1}$ from Fig. 2 by extrapolating the conductivities trend line to a null PVDF/CB ratio. Given a null PVDF concentration, the sensitivity of the parameter d is little since each particle has a high probability to be in direct contact with its neighbors. The effective value of 1900 $S\,m^{-1}$ is thus used to calibrate the material proportionality constant σ_0 by using a RVE with a CB jamming volume fraction of 0.64 and assuming an arbitrary unity tunneling range. Conductivity measurements of fluffy CB powder are usually performed on densified pellets subjected to high pressures. Since volume fraction information for the neat CB associated with the extrapolated conductivity is lacking, the jamming fraction is assumed. This assumption does not affect greatly the calibration process knowing that the conductivity of highly dense systems shows a relatively slight dependence on the volume fraction. This calibration task requires two runs only since the dependence of the effective conductivity on σ_0 is linear. A value of 312 $S\,m^{-2}$ is found. Conversely, as the PVDF content decreases below 1.22 and neat CB is approached, the conductivity decreases abruptly in the measured data. We believe that this is due to a loss of mechanical integrity in the lack of sufficient binding media. Extension of microcracks thus occurs in a large domain (relative to the RVE size) of several microns as experienced in [39,48]. This conductivity loss is thus believed to be a global phenomenon which is negligible inside our small scale RVE and the extrapolated trend in the near neat CB mixture remains valid in our analysis. The extrapolated σ_{eff}^{neat} value is moreover in agreement with the literature [44] where values between 1000 and 2000 $S\,m^{-1}$ are reported. The tunneling range is the remaining fitting parameter and is varied incrementally with a unit step from 1 nm. A value of 8 nm is found to result in a good fit which is also in agreement with reputed values (few nanometers).

For each of the four targeted PVDF/C volume ratios, five random equivalent microstructures are generated (one of which is plotted in Fig. 2) and the variance in conductivity due to the randomness

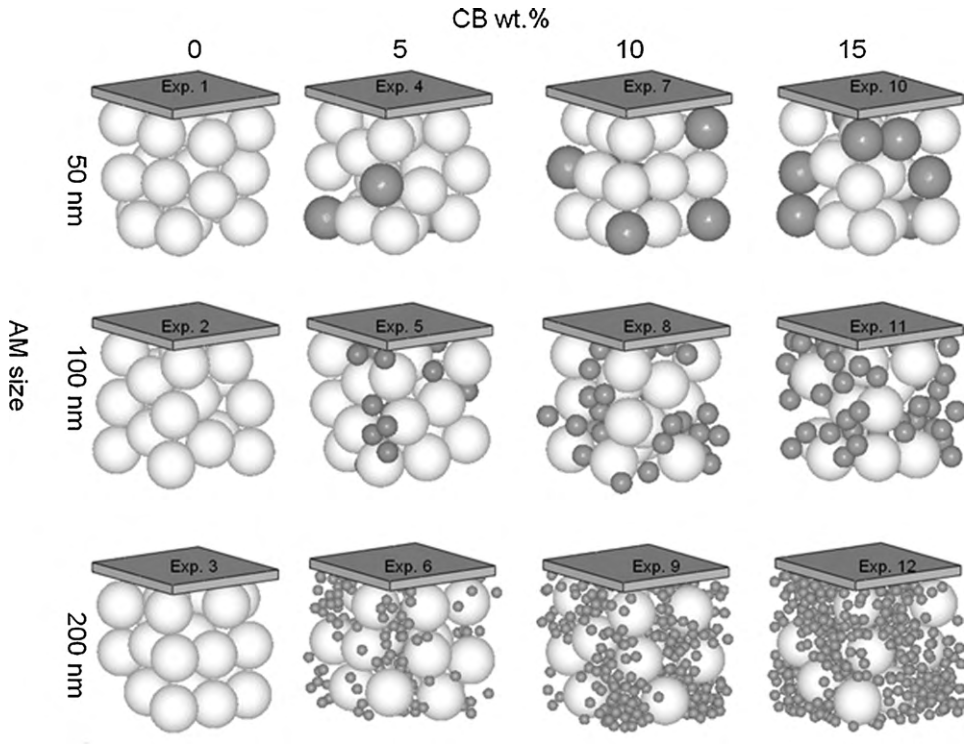

Fig. 3. Randomly generated microstructures for the considered CB wt.% and AM particle size factors.

feature of percolation is plotted in Fig. 2. As expected, the calculated variance increases with decreasing the CB vf.% but remains small enough not to affect the fit. Notice also how for CB vf.% less than the percolation threshold (29% for spheres), the electric transport is still achieved and similar in all five generated random structures. This is a direct effect of the tunneling phenomena which does not require the particles to be in touch making thus the percolation rule alone not valid.

6. Design of experiments

We dedicate this section to capture the variation of conductivity with the following factors:

1. nano-AM particle size;
2. CB particles wt.%;
3. carbon nano-coat (CNC) wt.%.

The modeling procedure shown in the previous section is used to perform a full factorial design of experiments (DoE) with three equidistant levels for the AM particle size (50, 100, and 200 nm) and carbon coating wt.% (0, 1, 3), and 4 equidistant levels for CB wt.% (0, 5, 10, 15) resulting in a total of 36 runs as listed in Table 1. The porosity is not a factor to be studied and fixed to 50%. The size of the RVE is fixed to three times that of the size of the AM particles which is above the minimum value reported to alleviate size effects [20]. The coating on the AM is assumed to be amorphous carbon with a uniform thickness and modeled as a layer of surface shell elements on top of the AM solid element faces. The variation in the coating wt.% and thus thickness is realized by varying the shell element thickness which is a property parameter. The electric potential in the thickness direction is assumed piecewise quadratic with 5 interpolation points. A conductivity of 1 e^{-08} S m^{-1} and density of 3.58 g cm^{-3} [20] is assumed for the bulk $LiFePO_4$. Fig. 3 shows all the 12 microstructures generated during this analysis.

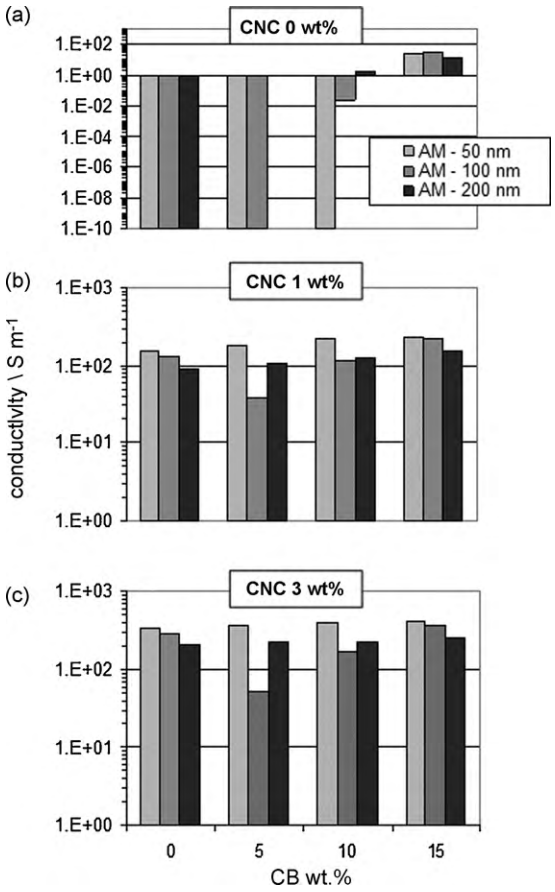

Fig. 4. Bar charts of achieved conductivities.

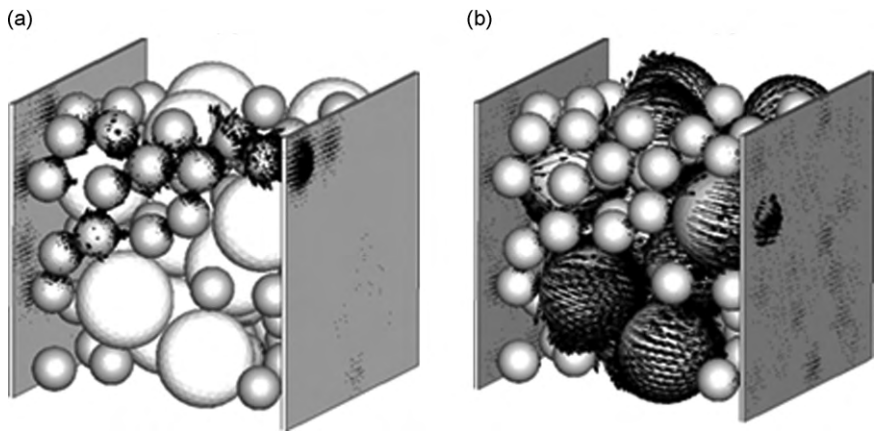

Fig. 5. A comparison of the electric transport in (a) bare AM-CB and (b) carbon coated AM–CB mixtures. The arrows are the current fluxes.

Important to mention is that the achievement of a conductive phase percolation is probabilistic due to the lower CB volume fractions. The conductivity may thus exhibit considerable variances for equivalent microstructures with the same weight ratios and porosity. In this work a probabilistic treatment is not in focus. Major jumps and trends in conductivities in widely different microstructures (Fig. 3) are sought rather than detailed comparative evaluations. The variances shown in [20], where similar porosities have been treated, can be seen small when we consider such a target allowing thus ourselves to base the analysis on a single generated random microstructure for each experiment.

7. Results and discussions

The conductivities calculated from the 36 experiments are listed in Table 1 and charted in Fig. 4. The achieved values of conductivities are somehow in the range of those reported in [49] and two order of magnitudes higher than those reported in [10]. The differences are obviously due to the lack of detailed microstructure modeling. Specifically, higher values are obtained in here due to the assumption that the AM have a uniform continuous carbon coating while in reality bare AM surfaces are possible [50].

The results are nevertheless valid for the following analysis.

7.1. Particle size effect

For bare AM (Fig. 4(a)), the particle size plays an important role. For the smallest 50 nm particles, percolation of CB conductive particles cannot be achieved before a 15 CB wt.%, while for the larger 100 nm and 200 nm particles percolation can already be achieved at 10 CB wt.%. This result can be implicated from Fig. 3. The small AM particles (50 nm) can separate easily the CB particles of similar sizes. An interconnected network is hardly probable. As the AM particle size increase finer CB particles reside in interstitial sites forming a structured interconnected conductive network which is uniformly distributed around the AM as elaborated in [17]. Increasing the AM particle size allows also more frequent AM–CB contacting enhancing thus Li+ insertion and local utilization while minimizing local stresses. Nevertheless, such a structure is not an easy task, especially when AM particles tend to be ultra fine, while tailored proprietary methods have been developed and patented [51]. The AM particle size seems not to have a noticeable influence in the existence of a CNC, which reminisces that ultra fine nanoparticles can be used to enhance diffusion as long as near uniform carbon coating exists.

7.2. CB addition effect

CB addition has its major effect on the bare AM by being the only conductivity deciding factor. A shift from 10% to 15% results in an improving factor of above 1000 in conductivity for the 100 nm bare particle sizes compared to a factor of 1.8 when a 1 wt.% CNC exists. For the carbon coated AM and for the bare AM beyond percolation level, the effect of CB addition is not drastic and a trend of conductivity stabilization can be observed.

7.3. Coating effect

The addition of a uniform CNC achieves suitable conductivities already with 1 wt.%, in the absence of any CB addition and for all particle sizes. This structure is an ideal case of a conductive phase surrounding the AM and forming interconnected network. The efficiency is obvious as a 3.5 wt.% carbon coating has been found equivalent in performance to 15 wt.% addition of carbon particles [6,8]. The dominant electric transport is through the CNC as elaborated in Fig. 5. Increasing the thickness of the coat do not account for a drastic change in conductivity. A change from 1% to 3% results in an utmost 2.3 factor of improvement in conductivities. In reality, as the coating increases, the sensitivity of the conductivity to the coating thickness decreases to zero and the conductivity faces a plateau. The CNC wt.% around which the plateau starts is found to be 5% in [50]. Nevertheless, even if the minimum amount of 1 wt.% is found theoretically sufficient, in experiments carbon loading below 1.5–2 wt.% are found to result in a non-continuous coating layer and carbon free AM surfaces which will affect the conductivity negatively [50].

8. Conclusion

In this work we have modeled the electrical conductivity of $LiFePO_4$ based composite Li-ion battery cathodes by an explicit representation of electrochemically active and conductive carbon particles. Such detailing level is currently needed given that the AM particles are tending towards ultra fine nanosizes (~30 nm) and carbon fillers can no longer be assumed as a continuum media. The inter-particle electric transport is achieved by modeling electric tunneling effects, which can be manifested by a contact clearance dependent resistance between nearby interacting points on different surfaces. The end conductivity is thus a result of a percolation–tunneling phenomenon. The model parameters have been identified by seeking a good fit to conductivity test data of a PVDF/C composite with varying mixing ratios. Besides higher accuracy, the advantages of such advanced modeling is the ability

to model the dependence of conductivity on mechanical aspects such as exerted pressures and AM particle deformations which are induced by the Li ion intercalation process.

A design of experiments has also been performed in order to capture the effects of AM particle sizes, CB wt.% and CNC wt.% on the effective conductivity. It has been found that in the absence of CNC, particle sizes and CB loading play a role in triggering conductivity. For the smallest AM particles (50 nm), the cathode acts as an insulator as long as the CB wt.% is below 15%. This threshold decreases to 10% with larger AM particle sizes (100 nm, 200 nm). The trend towards smaller AM particles to increase Li diffusion may conflict with gravimetric capacity if the CB increase does not lead to the activation of isolated AM. This is not the case when CNC is used. A value of 1 wt.% of uniform continuous CNC alone is sufficient to achieve practical conductivities for all particle sizes and in the absence of any conductive additives. The addition of more conductive materials, either as a coating or CB fillers, do not have a drastic effect on conductivity and may be avoided. Realizing a near continuous layer is thus a key to achieve high conductivity with minimum gravimetric capacity negative effects. Nevertheless, experiments have shown that a 1.5–2 wt.% of CNC is required to cover most of the AM particles, which raises slightly the theoretical threshold. The effect of continuous coating on Li ion diffusion and thus electrochemical cell behavior is also unknown and needs to be investigated. Once rendered conductive, the further addition of conductive additives has negligible effects on the rate capability of the cathode which is mainly controlled by Li transport. AM utilization could nevertheless increase and utilization modeling would be appropriate to further refine the selection of additive amounts.

Acknowledgement

This work is supported by the excellence initiative of the German federal and state governments whose members are greatly acknowledged.

References

[1] L. Gaines, R. Cuenca, Cost of lithium-ion batteries for vehicles, Argonne National Laboratory, Tech. Rep., 2000.
[2] A.K. Padhi, K.S. Nanjundaswamy, J.B. Goodenough, Journal of the Electrochemical Society 144 (1997).
[3] H. Kun Liu, G. Xiu Wang, Z. Ping Guo, J. Zhao Wang, K. Konstantinov, Journal of New Materials for Electrochemical Systems 10 (2007) 101–104.
[4] J.B. Goodenough, V. Manivannan, Denki Kagakuoyobi Kogyo Butsuri Kagaku 66 (1998) 1173.
[5] http://www.a123systems.com/a123/company (accessed 05.11.210).
[6] H. Huang, S.C. Yin, L.F. Nazar, Electrochemical and Solid State Letters 4 (2001) A170.
[7] R. Dominko, M. Gaberscek, J. Drofenik, M. Bele, J. Jamnik, Electrochimica Acta 48 (2003) 3079.
[8] Z.H. Chen, J.R. Dahn, Journal of the Electrochemical Society 149 (2002) A1184.
[9] R. Dominko, M. Gaberscek, J. Drofenik, M. Bele, S. Pejovnik, J. Jamnik, Journal of Power Sources 119 (2003) 770.
[10] C.-W. Wang, A.M. Sastry, K.A. Striebel, K. Zaghib, Journal of the Electrochemical Society 152 (5) (2005) A1001–A1010.
[11] K. Zaghib, J. Shim, A. Guerfi, P. Charest, K.A. Striebel, Electrochemical and Solid-State Letters 8 (4) (2005) A207–A210.
[12] S.Y. Chung, J.T. Bloking, Y.M. Chiang, Nature Materials 1 (2002) 123.
[13] N. Ravet, Y. Chouinard, J.F. Magnan, S. Besner, M. Gauthier, M. Armand, Journal of Power Sources 97 (2001) 503.
[14] J.D. Wilcox, M.M. Doeff, M. Marcinek, R. Kostecki, Journal of the Electrochemical Society 154 (2007) A389.
[15] S.S. Zhang, T.R. Jow, Journal of Power Sources 109 (2002) 72.
[16] J.K. Hong, J.H. Lee, S.M. Oh, Journal of Power Sources 111 (2002) 90.
[17] S. Ahn, Y. Kim, K. Joon Kim, T. Hyung Kim, H. Lee, M.H. Kim, Journal of Power Sources 81–82 (1999) 896–901.
[18] D. Guy, B. Lestriez, R. Bouchet, D. Guyomarda, Journal of the Electrochemical Society 153 (4) (2006) A679–A688.
[19] M. Gaberscek, J. Jamnik, Solid State Ionics 177 (2006) 2647–2651.
[20] Y.-H. Chen, C.-W. Wang, G. Liu, X.-Y. Song, V.S. Battaglia, A.M. Sastry, Journal of the Electrochemical Society 154 (10) (2007) A978–A986.
[21] D. Stauffer, A. Aharony, Introduction to the Percolation Theory, Taylor & Francis, 1994.
[22] E.K. Sichel, J.I. Gittleman, P. Sheng, The American Physical Society 18 (10) (1978) 5712–5716.
[23] Y. Wang, L. Zhang, Y. Fan, D. Jiang, L. An, Journal of Materials Science 44 (2009) 2814–2819.
[24] S. Vionnet-Menot, C. Grimaldi, T. Maeder, S. Strässler, P. Ryser, The American Physical Society, Physical Review B71 (2005) 064201.
[25] I. Balberg, The American Physical Society 59 (12) (1987) 1305–1308.
[26] C. Li, E.T. Thostenson, T.-W. Chou, American Institute of Physics, Applied Physics Letters 91 (2007) 223114.
[27] I. Balberg, D. Azulay, D. Toker, O. Millo, International Journal of Modern Physics B 18 (15) (2004) 2091–2121.
[28] M. Mundlein, J. Nicolics, Polytronic 2004 Presented at 4th IEEE International Conference on Polymers and Adhesives in Microelectronics and Photonics, 2004.
[29] Y.B. Yi, Acta Materialia 56 (2008) 2810–2818.
[30] S. Kari, H. Berger, U. Gabbert, Computational Materials Science 39 (2007) 198–204.
[31] R. Guises, Numerical simulation and characterisation of the packing of granular materials, Ph.D. Dissertation, Imperial College, London, United Kingdom, 2008.
[32] H.P. Zhu, Z.Y. Zhou, R.Y. Yang, A.B. Yu, Chemical Engineering Science 62 (2007) 3378–3396.
[33] H.P. Zhu, Z.Y. Zhou, R.Y. Yang, A.B. Yu, Chemical Engineering Science 63 (2008) 5728–5770.
[34] B. Rüger, J. Joos, T. Carraro, A. Weber, E. Ivers-Tiffée, The 216th Electrochemical Society Meeting, Vienna, Austria, 2009.
[35] A.M. Stux, D. Rowenhorst, D. Stephenson, J. Harb, D. Wheeler, The 214th Electrochemical Society Meeting, Honolulu, HI, 2008.
[36] M. Smith, R. Edwin García, Q.C. Horn, Journal of the Electrochemical Society 156 (11) (2009) A896–A904.
[37] K. Akemi Hirasawa, K. Nishioka, T. Sato, S. Yamaguchi, S. Mori, Journal of Power Sources 69 (1997) 97–102.
[38] M. Yoo, C.W. Frank, S. Mori, Chemistry of Materials 15 (2003) 850–861.
[39] G. Liu, H. Zheng, A.S. Simens, A.M. Minor, X. Song, V.S. Battaglia, Journal of the Electrochemical Society 154 (12) (2007) A1129–A1134.
[40] S. Babinec, H. Tang, A. Talik, S. Hughes, G. Meyers, Journal of Power Sources 174 (2007) 508–514.
[41] http://www.mathworks.com/products/matlab/ (accessed 05.11.2010).
[42] http://www.simulia.com/products/abaqus_fea.html (accessed 05.11.2010).
[43] G. Schwartz, S. Cerveny, A.J. Marzocca, Polymer 41 (2000) 6589–6595.
[44] M. Hindermann-Bischoff, F. Ehrburger-Dolle, Carbon 39 (2001) 375.
[45] J. Donnet, R.C. Bansal, M. Wang, Carbon Black, second ed., CRC Press, 1993.
[46] http://www.hypertextbook.com/facts/2007/DanaKlavansky.shtml (accessed 05.11.2010).
[47] H. Zhou, W. Peukert, Langmuir 24 (2008) 1459–1468.
[48] Z.P. Cai, Y. Liang, W.S. Li, L.D. Xing, Y.H. Liao, Journal of Power Sources 189 (2009) 547–551.
[49] S.L. Bewlay, K. Konstantinov, G.X. Wang, S.X. Dou, H.K. Liu, Materials Letters 58 (2004) 1788.
[50] J. Moskon, R. Dominko, R. Cerc-Korosec, M. Gaberscek, J. Jamnik, Journal of Power Sources 174 (2007) 683–688.
[51] R. Dominko, M. Gaberscek, J. Drofenik, M. Bele, S. Pejovnik, Electrochemical and Solid-State Letters 4 (11) (2001) A187–A190.